Preprint
UCRL-JC-136521

Biochemical Contributions to Corrosion of Carbon Steel and Alloy 22 in a Continual Flow System

J. Horn, S. Martin, B. Masterson and T. Lian

This article was submitted to
National Association of Corrosion Engineers
Corrosion '99
San Antonio, TX
April 25-30, 1999

U.S. Department of Energy

Lawrence
Livermore
National
Laboratory

December 3, 1999

BIOCHEMICAL CONTRIBUTIONS TO CORROSION OF CARBON STEEL AND ALLOY 22 IN A CONTINUAL FLOW SYSTEM

J. Horn, S. Martin, B. Masterson, and T. Lian
Lawrence Livermore National Laboratory, P.O. Box 808, Livermore, California 94550

ABSTRACT

Microbiologically influenced corrosion (MIC) may decrease the functional lifetime of nuclear waste packaging materials in the potential geologic repository at Yucca Mountain (YM), Nevada. Biochemical contributions to corrosion of package materials are being determined in reactors containing crushed repository-site rock with the endogenous microbial community, and candidate waste package materials. These systems are being continually supplied with simulated ground water. Periodically, bulk chemistries are analyzed on the system outflow, and surfacial chemistries are assessed on withdrawn material coupons. Both Fe and Mn dissolved from C1020 coupons under conditions that included the presence of YM microorganisms. Insoluble corrosion products remained in a reduced state at the coupon surface, indicating at least a localized anoxic condition; soluble reduced Mn and Fe were also detected in solution, while precipitated and spalled products were oxidized. Alloy 22 surfaces showed a layer of chrome oxide, almost certainly in the Cr(III) oxidation state, on microcosm-exposed coupons, while no soluble chrome was detected in solution. The results of these studies will be compared to identical testing on systems containing sterilized rock to generate, and ultimately predict, microbial contributions to waste package corrosion chemistries.

Keywords: Microbiologically Influenced Corrosion, MIC, Yucca Mountain, nuclear waste

INTRODUCTION

The U.S. Department of Energy has been assessing the suitability and design of a potential nuclear waste repository at Yucca Mountain (YM), Nevada. Native and introduced microorganisms in the repository environment may contribute to the corrosion of nuclear waste package (WP) materials. Microbiological contributions to WP corrosion must therefore be accounted for to accurately predict the time and mode of WP failure. Current efforts to predict corrosion of candidate WP materials over the long period required for containment of nuclear wastes have focused on modeling the chemical processes attendant to various corrosion modalities. Bacterial contributions to the corrosion chemistry of waste package materials are being assessed under conditions representative of those expected in the proposed repository environment. These determinations will then be factored into the overall model of waste package failure to better evaluate the degree of containment afforded by waste packages.

Simulation of a saturated, oxic WP environment (intended to mimic re-entry of YM ground water into the repository drifts) was achieved in a continual-flowthrough reactor (or, "microcosm") fed with a synthetic groundwater formulation. The apparatus contained sterilized candidate WP material coupons and crushed YM rock in a non-sterilized condition (i.e., containing the microorganisms from the post-construction repository environment), or pre-sterilized. Periodically, the chemistry of the dissolved ions in the aqueous reactor efflux were analyzed. Precipitated corrosion products attached to withdrawn material coupons, along with spalled corrosion products were also assessed and quantified. These collective data provide the identification of corrosion products and establish their rates of formation, which can be modeled to supplement a general corrosion code. Speciation of corrosion products will also aid in determining their abilities to adsorb or transform radionuclides. Gravimetric measurements of coupon weight-loss were additionally performed to supply overall rates of corrosion. Comparison of results from systems containing non-sterile YM rock with those results obtained from systems with sterilized rock will provide the microbial contributions to determine rate constants, overall corrosion rates, and the species of observed corrosion products.

Here, we present preliminary results of these studies with two candidate WP materials, carbon steel C1020 (C1020, UNS G10200). and Alloy 22 (UNS N06022), from non-sterile systems.

APPROACH AND EXPERIMENTAL METHODS

Microcosm Reactor Components

The microcosm apparatus (Fig. 1), a continuous flow-through system, consisted of a borosilicate glass vessel (500 mL) fitted with an inlet for introducing synthetic YM ground water (below) from a 2 liter reservoir, and an outlet for draining the spent media. The influx and efflux rates were maintained at an equivalent, constant rate (2 mL/hr) with the aid of peristaltic pumps, to maintain a volume of 250 mL of ground water in the vessel (total residence time was approximately 5 days). In-line media break tubes were incorporated into the outlet tubing to prevent back-contamination, and in-line filters (0.2 µm) were included on the inlet tubing to assure sterility of introduced synthetic ground water. All components of the system were pre-sterilized, and the sterility of those system elements upstream of the microcosm vessel were maintained and monitored by live plating techniques[1]. Reactors were incubated for a total of three months at ambient laboratory temperature, approximately 22° C.

Synthetic ground water (10XJ13 media) was formulated from a ten-fold concentration of YM ground water (well J13 in the YM region[2]) using *The Geochemist's Workbench* [3] (Table 1). The ionic strength of the synthetic groundwater was increased ten-fold to mimic the anticipated increased concentration of groundwaters entering the proposed repository. To prevent precipitation of minerals due to concentrating the reported ground water composition, and control initial pH, the concentrations of calcium, sodium, and carbonate were decreased (with respect to the reported composition of J13), resulting in near-saturation conditions with respect to mineral phases (Table 1). Additionally, the 10XJ13 media was supplemented with 0.1% glucose, a minimal organic carbon source; the final pH was 7.6. Previous studies had shown that this formulation supported microbial growth of organisms contained in YM rock[4]. Available forms of soluble silica (metasilicates) significantly increase the pH of the solution, therefore no silica was added to the synthetic 10XJ13 formula; silica was only thus provided from dissolution of the added YM tuff (below).

In addition to synthetic ground water, completed microcosms each contained 20 candidate waste package material coupons [either C1020 or Alloy 22 (Table 2)]; 12.7 cm^2 surface area per coupon, total coupon surface area was 254 cm^2 per microcosm reactor] imbedded vertically in crushed YM rock (100 g); coupons were placed to prevent physical contact between them. Coupons were either placed in reactors containing non-sterilized or pre-sterilized YM rock (below), to permit evaluation of microbiological contributions to observed results. The material coupons were prepared by stamping with identification numbers, wet-polished with abrasive paper progressively to 600-grit, and cleaned with distilled water and acetone. Coupons were then weighed for eventual weight-loss analysis before being sterilized (using a ^{60}Co gamma source, 3-4 Mrad total dose)[5], and emplaced in constructed microcosms using sterile techniques. In addition to the metal coupon-containing microcosms, reactors without coupons were assembled to assess the effects of YM rock on ground water chemistry.

YM volcanic welded tuff was aseptically collected from the drift walls of the Exploratory Study Facility (ESF,YM, Nevada) in a region of the repository horizon geologic strata (adjacent to Alcove 5). Collected tuff was then crushed and sieved (particle size fraction 1-4 mm) using sterile techniques, and stored under sterile conditions, to prevent contamination with microorganisms not associated with post-construction repository conditions. YM tuff composition[6] is shown in Table 3. To assess the effects of abiotic corrosion, in parallel experiments, aliquots of tuff were sterilized (3-4 Mrad gamma irradiation, as above). Gamma doses of 3 Mrad were sufficient for eradicating the most recalcitrant organisms, while preventing alteration of the tuff composition[5].

The various microcosm permutations (one of two materials types, or no materials) were performed in duplicate.

Sample Collection and Preparative Techniques

Material Coupons. C1020 and Alloy 22 coupons were removed from their respective microcosms using sterile techniques, after which a single coupon from each microcosm was immediately fixed in a 2% gluteraldehyde solution for scanning electron microscopy and energy dispersive spectral analysis (SEM/EDS). Additionally, two coupons of each material were immediately dried under N_2 gas and placed in a N_2-purged desicator for storage until analyzed by x-ray diffraction (XRD) and inductively coupled plasma atomic emission spectrometry (ICP-AES) of removed corrosion products. Coupons were initially x-rayed *in situ*. Then, to prevent interference with signal originating from the underlying uncorroded coupon surface by penetration of the x-ray beam through the corroded layer, adhered corrosion products were scraped from the surface, lightly ground, suspended in de-ionized water, dropped onto a quartz plate, and subjected to XRD. Scraped and collected corrosion products from a single coupon were also dissolved in 20 mL of HCl-acidified water (pH 2) and analyzed by ICP-AES to provide quantitative elemental compositions. Finally, a single C1020 coupon was oven dried under oxic conditions at 50 °C to compare the effects of preparative conditions on subsequent analytical results. Unreacted/unexposed material surfaces were analyzed in parallel with those withdrawn from microcosms to assess the corrosive effects under experimental microcosm conditions.

Bulk Solution. Periodically, aliquots of bulk aqueous solution effluxed from microcosm reactors were collected and filtered (0.2 µm) at the reactor outlet. An aliquot was subjected to analysis of pH, then the remaining sample was acidified to pH 2 with HCl to maintain the solubility of contained ions before being analyzed by ICP-AES. Transition metals, alkali earth metals, and alkali metals relevant to material coupon composition (Table 2) were quantified.

Spalled and Precipitated Corrosion Products. Particulates (either spalled or precipitated) not attached to test coupon surfaces were removed from a non-sterile C1020-containing microcosm (no material coupons had previously been removed). First, coupons were removed and the bulk solution decanted. Then, particulates attached to the crushed tuff and microcosm walls were ultrasonically removed (Heat Systems Ultrasonics, Model W185 Sonifier, setting 4, 2 min. pulse), added to the decanted mother liquor, and pooled particulates were allowed to settle. The resulting slurry of particulates was agitated to homogenize the mixture, dropped onto a quartz plate, and air dried for XRD analysis. A second aliquot was removed, filtered (0.2µm), the solids were gently scraped from the filter and dissolved in an HCl solution (pH2) for subsequent ICP-AES analysis.

Analtyical Techniques

XRD. Powder XRD analysis was used to identify crystalline phases, 1) *in* situ, on coupon surfaces, 2) scraped and homogenized from coupon surfaces, and 3) spalled and precipitated particulates collected as described. Samples were x-rayed using a diffractometer (Scintag, PAD V) with Cu-Ka radiation coupled to a SiLi solid state detector. Scanning parameters were 2-70° 2-theta, 0.02 degrees/step, 1-2 sec/step, 45 kV, and 35mA. X-ray generator slits were set at 1° and 2°, and detector slits were set at 0.3 mm and 0.2 mm. Finally, an important caveat to this technique is XRD analysis is not a practical tool for identifying phases that are present at less than a few wt %.

SEM/EDS. Material coupon surfaces were characterized with a field emission scanning electron microscope (Hitachi S-800) equipped with a Kevex 8000 microanalysis system for image and elemental analyses, respectively. The effective electron beam probe depth was 1 µm. The coupons were coated with carbon to reduce electrical charging of non-conductive materials. Operating parameters for imaging and energy dispersive spectral analysis (EDS) were 16KV accelerating voltage, 0-10.23 keV range, approximately 1500 cts/sec, and <20% deadtime. The beam was cropped or operated in spot mode during elemental analysis.

ICP-AES. Concentrations of those elements relevant to the composition of test coupons (Table 2) were analyzed in bulk aqueous reactor effluents using ICP-AES (Applied Research Laboratories, Model 3560 equipped with a simultaneous optical system, Rowland Circle). Parameters of analysis were: incident power, 1150KW; net gas flow rate, 0.4 L/min; plasma gas flow rate, 16 L/min; reflected power, <2 KW. Fe and Mn concentrations were measured on samples collected from the C1020 microcosms; Co, Cr, Fe, Mn, Mo, Ni, V, and W on samples collected from Alloy 22-containing microcosms. These elements were also analyzed in solution samples collected from no-metal control microcosms to ascertain the concentration of these elements that are contributed by either the synthetic 10XJ13 or solubilized YM rock components.

RESULTS

Dissolution of Material Coupons:Analyses of Aqueous Reactor Effluents

The original pH of synthesized 10XJ13 fed into the microcosms was approximately 7.6; after incubating for the requisite five day residence time in all reactors the pH remained within $\pm$ 0.2 pH units of 7.6, and remained within this range during the entire three month period of incubation.

Comparison of solubilized Fe and Mn concentrations in the C1020-containing microcosms with those concentrations in the no-metal control reactors by ICP-AES analysis are shown in Fig. 2. The concentration of Fe in solution in C1020 microcosms initially was approximately 10 ppb, then increased to an average of 100 ppb after 90 days of incubation. Concentrations of Fe in the microcosms containing no coupons remained below detection limits. Soluble Mn concentrations in C1020-containing microcosms increased by an even greater degree than Fe over the three month course of incubation: initially the concentration of Mn was below detection limits and it rose to 700 ppb during the 90 days of incubation. In comparison, Mn concentrations remained low (< 60 ppb) in effluents from microcosms containing no material coupons (Fig. 2).

Only Mn was consistently detected in bulk efflux solutions from microcosms containing Alloy 22, however, no metal control microcosm efflux samples increased to the same degree (approximately 60 ppb) over the course of incubation (Fig. 3). All other alloying components of Alloy 22 (Table 2) were undetectable. Iron concentrations were generally below the detection limit except for a single increase in one alloy-containing microcosm after 65 days, probably reflecting experimental variation in the data.

Coupon-Adhered Corrosion Products

C1020. SEM image analysis of a glutaraldehyde-fixed C1020 coupon after three months exposure in the microcosm environment showed a thick, fractured, heterogeneous film overlaying the metal surface. The morphology of the underlying metal surface, which was observed at places where the film had broken using SEM, revealed isometric-shaped crystals which EDS analysis revealed contained Fe and Mn, consistent with the carbide primary structure of carbon steel (Table 2); subsequent XRD analysis showed these regions to contain cohenite. Thus, etching of the surface had occurred during incubation, because unexposed coupons did not display the same morphology (Fig 4). The heterogeneous morphology of the thick film indicated the formation of several phases. At higher magnification book-like rhombohedrons were identified with EDS as composed of

Ca and O, and were identified as calcite (calcium carbonate) crystals by XRD. Rod shaped bacteria were attached to the outer edges of the rhombs (Fig. 4, 5). A second morphological phase, as revealed by SEM, was reminiscent of angular honeycombs with an inward spiral (Fig. 5). EDS analysis showed these particles were predominantly composed of Fe, Si, and O and a minor amount of Al. A third morphological phase consisted of cable-like crystals centrally attached in a bundle and identified with elemental analysis as Ca, Si, and O (Fig. 5). The penetration of the electron beam through the film coating and into the coupon surface resulted in the presence of large Fe peaks in most EDS spectra. Silicon peaks were also observed in many of the spectra, probably due to the presence of amorphous silica (dissolved from the tuff), which is likely to form at ambient temperatures in siliceous systems[7].

XRD analysis indicated that untreated, unexposed C1020 coupon surfaces contained only elemental iron. Manganese, present at 0.47 wt% in C1020, was below the detection limits of this technique. In contrast, the *in situ* XRD analysis of the N_2-dried C1020 coupon indicated that the coupon surface was composed of elemental iron, cohenite (Fe_3C), calcite ($CaCO_3$), a greenalite-like phase [$Fe_3Si_2O_5(OH)_4$, 1:1 Fe(II) layer silicate], and rancieite [$(Ca,Mn)Mn_4O_9{\cdot}3H_20$], a manganese phase commonly co-occurring with iron oxides. A small, broad amorphous peak was also noted in the XRD spectrum, probably due to an amorphous silica phase. These data, taken together with the SEM/EDS analyses, strongly suggest that the rhombohedron structures (with adhered bacteria) are in fact calcite crystals, the greenalite crystals are the spiraled angular honeycomb structures, and the cable-like forms are an unidentified mineral phase. The elemental composition of rancieite (identified by XRD analysis) was not observed using EDS. These results are summarized in Table 4.

XRD analysis of the material scraped from the N_2-dried coupon indicated that only the greenalite-like mineral and calcite were present. Rancieite was not detected, but may have been present in too minor an amount (especially if some of this mineral was lost in sample preparation) to detect with XRD. However, ICP analysis of this scraped material did show both Mn and Ca, both elements contained in rancieite. In general, those elements detected in the scraped material by ICP showed good agreement with those detected using both XRD and EDS analyses. Further, the quantity of each element detected on single coupons by ICP quantitatively delineates the accumulation of adhered corrosion products and those species precipitated from solution.

In situ XRD analysis of the C1020 coupon dried in an oven under oxic conditions indicated that calcite, elemental iron, goethite (FeO(OH)), and lepidocrocite (FeO(OH)), as well as greenalite were present. Goethite and lepidocrocite both contain iron in the oxidized Fe(III) state, while greenalite contains ferrous [Fe(II)] iron. Iron phases were thus present in both the ferric and ferrous forms, unlike those observed (i.e., only greenalite) when coupons were dried under anoxic conditions. It is therefore likely that some of greenalite was oxidized to goethite and lepidocrocite on oven drying in an oxygenated environment.

Alloy 22. Initial SEM image analysis at low magnification (50X) of microcosm-exposed, glutaraldehyde-fixed Alloy 22 after three months exposure in the microcosm environment showed a partially coated coupon surface. The coating was homogeneous and composed of tightly packed hemispherical particles when inspected under higher magnifications (>600X). EDS analysis of this coating demonstrated that the hemispherical particles were composed of Cr and O (Fig. 6, 7). In contrast, unexposed/unincubated Alloy 22 showed a polished, uncoated surface without any hemispherical particles (Fig. 6). The portions of the exposed coupon that remained uncoated (appearing at breaks in the coating), was similar in morphology and elemental composition (W, Mo, Ni, Cr, Fe, and V) to unreacted Alloy 22 (Table 2). Angular particles scattered on these uncoated coupon surfaces (Fig. 6) were composed of Al, Si, K, Na, and Ca, suggestive of a tuff feldspar fines; not a precipitated phase, nor originating from corrosion of the alloy.

XRD analysis of the unreacted Alloy 22 metal coupon surface indicated that it contained Ni-Cr-Co-Mo metal[8], consistent with the composition of the alloy. When a microcosm-exposed, unfixed Alloy 22 coupon was examined with XRD, the spectra showed that it remained unaltered after exposure in the microcosm; the spectra was identical to the unexposed coupon. There was no XRD evidence of the chrome-enriched coating (visualized with SEM/EDS, above) when the coupon was not pre-fixed with glutaraldehyde. Further, subsequent SEM analysis of this unfixed coupon showed no evidence of the presence of the coating. Loss of the coating was probably due to its loose adherence to the coupon surface and subsequent spallation; glutaraldehyde fixation was most probably required to detect the presence of the coating.

Analysis of Spalled and Precipitated Particulates from a C1020 microcosm

XRD analysis of the particulates harvested from the microcosm were composed of lepidocrocite [FeO(OH)], goethite [FeO(OH)], smectite (a layered aliminium or magnesium silicate), cristobalite (SiO_2), and several feldspars, probably microcline, sanidine, and/or calcium-bearing albite (potassium, sodium, or calcium aluminosilicates). ICP-AES analysis of these particulates indicated that they were composed of Fe, Si, Ca, Al, Mn, K in descending order of concentration. Smectites are present in small concentrations in YM tuff, therefore their presence in the particulate phase (and their composition) indicates that they originate from the tuff or were formed as a secondary phase in the 10XJ13 media, and are not corrosion products. Cristobalite and feldspars are also minerals associated with YM tuff. Only the lepidocrocite and goethite are probable corrosion products; both of these contain Fe in the Fe(III) oxidation state.

DISCUSSION

The aim of this effort was to determine the chemical contributions of microorganisms likely to be found in the potential YM repository on corrosion of nuclear waste package materials. Our approach implements a system that includes the central elements of the repository: rock, ground water, and waste package materials, in a continual-flow system meant to mimic re-entry of subsurface waters into the repository drifts. Analyses of the chemistry of the system (with special attention to the degradation of the introduced material compositions) in the aqueous, surfacial, and particulate fractions of the system permits chemical alterations of the system to be determined over time; thus, both rates and chemical mechanisms may be deduced. Further, characterization of corrosion products will aid in assessing whether they will participate in downstream events which may effect containment of nuclear wastes, for example the adsorption of radionuclides to specific corrosion products. Finally, comparison of results from systems containing microorganisms obtained from the post-construction repository environment to those which have been sterilized (but are otherwise identical), will show microbial contributions to corrosion chemistry. Here, we report preliminary results during a three month incubation period from non-sterile reactor systems; analysis of coupons from sterile reactors is ongoing, and incubation of all reactors is proceeding to evaluate longer-term effects.

C1020

Elemental iron and cohenite observed in XRD spectra of microcosm-incubated, N_2-dried C1020 are consistent with the basic crystal structure of carbon steel. However, cohenite was not observed on unexposed/unreacted coupons, indicating that the protective oxide layer present on unexposed coupons had been etched away during exposure in the microcosm environment (Fig. 4). Calcium carbonate crystals observed on the incubated C1020 coupons were generated from Ca contained in the 10XJ13 medium and/or dissolved from tuff, reacting with carbonate (also a 10XJ13 component, and available atmospherically); these are the only sources of calcium and carbonate in the system. Bacteria were observed only associated with one facet of these calcite crystals (Fig. 4, 5), possibly inferring electrostatic interactions between the bacterial surface and a given crystal face. No bacteria were observed directly on the coupon surface at this point (three months) of incubation. Previously, it has been reported that biofilms on Nickel-Chrome alloys trapped inorganics in solution, leading to the nucleation of calcite formation; eventually crevices were formed by accumulated calcite where breakdown of the passive oxide layer occurred [9]. This type of under-deposit/crevice mode of corrosion may be observed as the incubation of this system progresses.

SEM/EDS analyses were critical in identifying the mineral phases identified with XRD analyses, as summarized in Table 4. Our analytical strategy focused on imaging specimen surfaces with associated corrosion and other products using SEM, using EDS to assess elemental compositions of features visualized by SEM, and then assessing their minerology and oxidation state by XRD analysis. The rhombohedrons composed of Ca and O are very likely calcite crystals. The honeycomb phase containing Fe, Si, O with a small amount of Al is probably the greenalite-like mineral. The presence of Al in the EDS spectrum may indicate a substitution of Al (possibly arising from tuff) for Fe in this phase, as described by Floran[10]. Additionally, the sample mounting stub is composed of aluminum and could have contributed to Al in the EDS spectrum. The cable-like phase composed of Ca, Si, and O is an unidentified calcium silicate mineral not observed in the XRD pattern possibly due to its presence in insignificant concentrations, but which, due to its elemental composition, evidently

originates from the YM tuff and 10XJ13. Rancieite, while not identified by EDS in the SEM images, also appeared to be a present in minor amounts, because it was lost when coupons were scraped; and it appears that most of the dissolved Mn from tuff stayed in solution (Fig. 2).

YM tuff contains minor amounts of Fe(III) and Mn (Table 3). It is unlikely that Fe(III) or manganese oxides contained in tuff were dissolved at the neutral pH and generally oxygenated conditions extant in the microcosm environment. This contention is supported by the observation that Fe and the bulk of the Mn detected in solution were dissolving from C1020 coupons in the reactor environment (Fig. 2). Thus, it is evident that Fe(II) detected on coupons in the form of greenalite, and the Mn associated with rancieite, both derived from dissolution of C1020. The only source of silica, including that associated with the formation of greenalite, was that dissolved from tuff. Further, the formation of an Fe(II) phase (greenalite) strongly suggests that a reduced environment exists at least locally at the coupon surface, as it appears likely that the greenalite phase was present on the coupon surface before the coupons were dried (goethite and lepidocrocite, both Fe(III) phases were observed on coupon surfaces only after drying under oxygenated conditions). In fact, the presence of biofilms on surfaces is known to result in the formation of oxygen gradients, with a depletion of oxygen closest to the metal surface through microbial respiration[11]. Given that the Fe and Mn measured in samples collected from bulk solutions, precipitates, and scraped corrosion products were generated from dissolution of the C1020 coupon, these quantitative ICP data provide a means of generating chemical corrosion rate expressions.

Bulk solution particulates analyzed with XRD contained Fe(III)-bearing oxyhydroxides, which again, must have originated from solubilized coupons (because no Fe was observed to have been solubilized from tuff, Fig. 2). These Fe precipitates were oxidized, indicating that oxygen was present in the bulk solution (note that air was able to enter the media reservoirs), however, given the concentrations of soluble (reduced) Fe and Mn in the C1020-containing bulk solutions, it is possible that the concentration of soluble oxygen was not great enough to oxidize (and precipitate) all the Mn and Fe present. Further, binding of oxygen by dissolved Fe and Mn clearly contributes to depletion of oxygen in the bulk environment. An oxygen gradient may also quite likely exist whereby the oxygen concentration is higher at the waterline and lower at the coupon/tuff stratum. Similarly, while the pH of microcosm effluent samples remain unchanged, a localized alteration in pH could exist on coupon surfaces. Miniaturized oxygen and pH probes will be used in future sampling to resolve these issues. It should also be noted that precipitate samples were initially air-dried, thus it is likely that any reduced iron phases were oxidized on sample preparation, though nitrogen-dried particulates that were recently analyzed with XRD did reveal the same assemblage of mineral phases as the air-dried preparation. Given the present data though, it appears that attached iron corrosion products remain in a reduced form, while those that spall or are precipitated from solution are oxidized, and substantial amount of solubilized metal remains in solution in a reduced form.

Comparison of the coupon drying techniques, oxic oven and N_2-dried, indicate that they share three phases; calcite, iron, and the greenalite-like phase. Cohenite was not seen in the oven-dried sample probably due to the heavy iron oxide coating that developed during heating. Some of the reduced iron greenalite phase remained after heating at 50° C., indicating that this mineral is somewhat recalcitrant to oxidation at this elevated temperature. However, other Fe-bearing phases observed on the oven-dried coupon were oxidized, namely, goethite and lepidocrocite. Nitrogen-drying thus allowed the phases that formed on the coupon surface in the microcosm to remain intact, without the formation of other artifactual oxidized mineral phases due to drying coupons under oxic conditions and is, therefore, more representative of the *in situ* saturated microcosm environment.

Alloy 22

SEM/EDS analyses of a microcosm-exposed, glutaradelhyde-fixed Alloy 22 coupon surface showed a chrome oxide layer composed of hemispherical particles; these were not observed on unexposed coupons (Fig. 5). While unexposed coupons were also unfixed, it is highly unlikely that glutaraldehyde fixation caused the creation of the chrome oxide deposit; to unequivocally determine that this chrome oxide layer is not a fixation artifact, unexposed coupons are currently being fixed and analyzed by SEM. This chrome oxide layer was apparently very loosely adhered to the coupon surface, since when coupons were unfixed and analyzed by XRD or re-analyzed by SEM/EDS, it had been lost by spallation. Despite the presence of this chrome oxide layer,

microcosm-incubated coupons showed no immediate grossly visible signs of corrosion or surfacial coatings upon sampling.

Soluble chromium [Cr(VI)] was not detected in bulk solution samples analyzed with ICP-AES. The other common oxidation state of Cr, Cr(III) is highly insoluble under oxidizing conditions at circumneutral pH and ambient temperature, indicating that the chrome oxide layer observed on microcosm-exposed Alloy 22 is almost certainly a Cr(III) oxide or hydroxide. It is therefore plausible that chrome originating from dissolution of the Alloy 22 went into solution as Cr(II), which spontaneously oxidizes to Cr(III) and then precipitated as a Cr(III) oxide, coating the coupon surface. Other investigators have noted that Alloy 22 surfaces become enriched in tungsten and molybdenum under acidified conditions[12], and previous studies show preferential dissolution of chrome from Alloy 22 in the presence of bacteria under alternative conditions from those used here[13,14]; these findings are consistent with a loss of chrome during corrosion of Alloy 22 under the microcosm conditions described here.

ICP-AES analysis of the solubilized Fe and Mn concentrations in microcosms containing Alloy 22 indicated that there was no increase when compared with the no-metal-containing controls. The minor amount of Mn in solution originates from dissolution of the YM rock in the system. Clearly, no Mn or Fe was observed to have corroded from Alloy 22 coupons.

Conclusions

Here, we have used a combination of analytical techniques, including SEM/EDS and XRD to determine the identity of corrosion products; ICP has been used to quantify these solids and to quantify soluble corrosion products in the aqueous phase. Although it was not known *a priori* whether crystalline or amorphous corrosion phases would form, XRD (which only detects crystalline products) was applied. Fortunately, this technique proved useful in the case of C1020 analysis, because most of the phases were crystallized; although a minimal quantity of amorphous corrosion material was observed. It was found that both Fe and Mn dissolved from C1020 coupons under representative repository conditions that included the presence of YM microorganisms. Insoluble corrosion products remained in a reduced state at the coupon surface, indicating at least a localized anoxic condition; soluble reduced Mn and Fe were also detected in solution, while precipitated and spalled products were oxidized. Alloy 22 surfaces showed a layer of chrome oxide, almost certainly in the Cr(III) oxidation state, on microcosm-exposed coupons, while no soluble chrome was detected in solution. The contribution of the microorganisms contained in these systems awaits the analysis of sterile control systems, which is currently in progress. Further, all microcosms are continuing to be incubated so that accurate dissolution rates of metals by quantification of analyzed corrosion products can be determined over a longer incubation period. Overall corrosion rates as determined by weight-loss measurements are also being undertaken.

ACKNOWLEDGMENTS

The authors wish to gratefully acknowledge expert technical assistance provided by Michael Davis, Angel Rivera, and Anabel Miranda in performing these experiments. This work was performed under the auspices of the U.S. Dept. of Energy by Lawrence Livermore National Laboratory under contract W-7405-ENG-48, and was supported by the Yucca Mountain Site Characterization Project, LLNL.

REFERENCES

1. T.D. Brock, M.T. Madigan, Biology of Microorganisms, (Englewood Cliffs, NJ: Prentice Hall, 1991): p. 310-311.

2. J.M. Delany, Reaction of Topopah Spring Tuff with Water: A Geochemical Modeling Approach Using the EQ3/6 Reaction Path Code, Lawrence Livermore National Laboratory report, UCID-53631, November, 1985.

3. C.M. Bethke, The Geochemist's Workbench, Version 2.0: A Users Guide to Rxn, Tact, React, and Grplot (Illinois: University of Illinois Hydrogeology Program, 1994).

4. R. Daniel McCright, Engineered Materials Characterization Report, volume 3, Corrosion Data and Modeling Update for Viability Assessment, Lawrence Livermore National Laboratory report, UCRL-ID-119564, September 1998.

5. J.T. Trevors, Journal of Microbiological Methods, 26(1996):p. 53.

6. D.E. Broxton, D.L. Bish, R.G. Warren, Clays and Clay Minerals, 35, (1987): pp. 89-110.

7. S. Carroll, E. Mroczek, M. Alai, M. Egbert, Geochimica et Cosmochimica Acta, 62(1998): p.1379.

8. Powder Diffraction File, PDF-2, Database Sets 1-46, Inorganics, International Centre for Diffraction Data, Pennsylvania (1996).

9. A.M. Brennenstuhl, P.E. Doherty, P.J. King, and T.J. Dunstall, Microbially Influenced Corrosion and Biodeterioration. (Knoxville, TN:The University of Tennesee Press, 1990): pp. 4-25-4-31.

10. R.J. Floran, J.J. Papike, Bull. Geol. Soc. Am., 86(1975): p. 1169.

11. S.W. Borenstein, Microbiologically Influenced Corrosion Handbook, (New York, New York: Industrial Press, 1994): p. 146.

12. Joseph Farmer, personal communication.

13. G.G. Geesey, R.J. Gillis, R. Avci, D. Daly, M. Hamilton, P. Shope, G. Harkin, Corrosion Science, 38(1996): p. 73.

14. T, Lian, D. Jones, S. Martin, J. Horn, “A Quantitative Assesment of Microbiological Contributions to Corrosion of Candidate Nuclear Waste Package Materials,” Materials Research Society Fall Meeting, (Boston, MA:Material Research Society, 1998).

Table 1. Comparison of natural J13 ground water (concentrated 10-fold) with synthetic J13 water (concentrated 10-fold)

	10X J13* ground water	10X J13 synthetic water
component	*concentration, mM*	*concentration, mM*
Na	19.100	6.143
K	1.310	1.306
Ca	3.120	2.505e-2
Mg	0.790	0.790
NO3	1.550	1.553
Cl	1.950	1.951
CO3	20.500	0.527
SO4	1.950	1.949
Li	0.061	0
Sr	0.004	0
Al	0.004	0
Fe	0.001	0
Si	9.610	0
F	1.160	1.160
Glucose	0	5.550

*J.M. Delany, "Reaction of Topopah Spring Tuff with J-13 Water: A Geo-chemical Modeling Approach Using EQ3/6 Reaction Path Code," UCID-53631, Lawrence Livermore National Laboratory, (1985).); reported concentrations were increased ten-fold to approximate increased ionic strength due to anticipated repository effects.

Table 2. Compositions of carbon steel 1020 and Alloy 22 coupons

Alloy	*C (wt%)*	*Mn (wt%)*	*P (wt%)*	*S (wt%)*	*Fe (wt%)*	*Co (wt%)*	*Mo (wt%)*	*Si (wt%)*	*Cr (wt%)*	*W (wt%)*	*V (wt%)*	*Ni (wt%)*
C1020	0.20	0.47	0.012	0.013	bal							
Alloy 22	0.002	0.260	0.012	0.001	3.950	0.510	13.400	0.025	21.580	2.820	0.150	bal

Table 3. Bulk-rock compositions for Topopah Spring tuff atYucca Mountain, Nevada*

	Unaltered lower vitrophyre	Altered lower vitrophyre
Element	concentration, wt%	concentration, wt%
Si	72.2	69.6
Ti	0.07	0.10
Al	14.3	19.5
Fe^{3+}	0.78	1.07
Mn	0.05	0.06
Mg	0.45	1.33
Ca	0.69	3.73
Na	6.43	3.65
K	4.98	0.91
P	0.01	0.02

*D.E. Broxton, D.L. Bish, R.G. Warren, Clays and Clay Minerals, 35(1987): p. 89. Rock used was from the repository geological horizon, and was devitrified, however compositionally it is identical to that reported for vitrified rock.

Table 4. Solid Phase Analyses of Microcosm-Exposed C1020

Gluteraldehyde-dried		Nitrogen-dried	
SEM	**EDS**	***in-situ* XRD**	**Scraped XRD**
pyramidal-shaped	Fe, Mn	Cohenite (Fe_3C)	substrate
rhombohedrons	Ca, O	calcite ($CaCO_3$)	calcite
honeycombs	Ca, Si, O	Greenalite($Fe_3Si_2O_5(OH)_4$	greenalite
cables	Si, O, Fe (Al)	—	—
—	—	rancieite ((Ca, Mn)Mn_4O9 $3H_2O$)	—

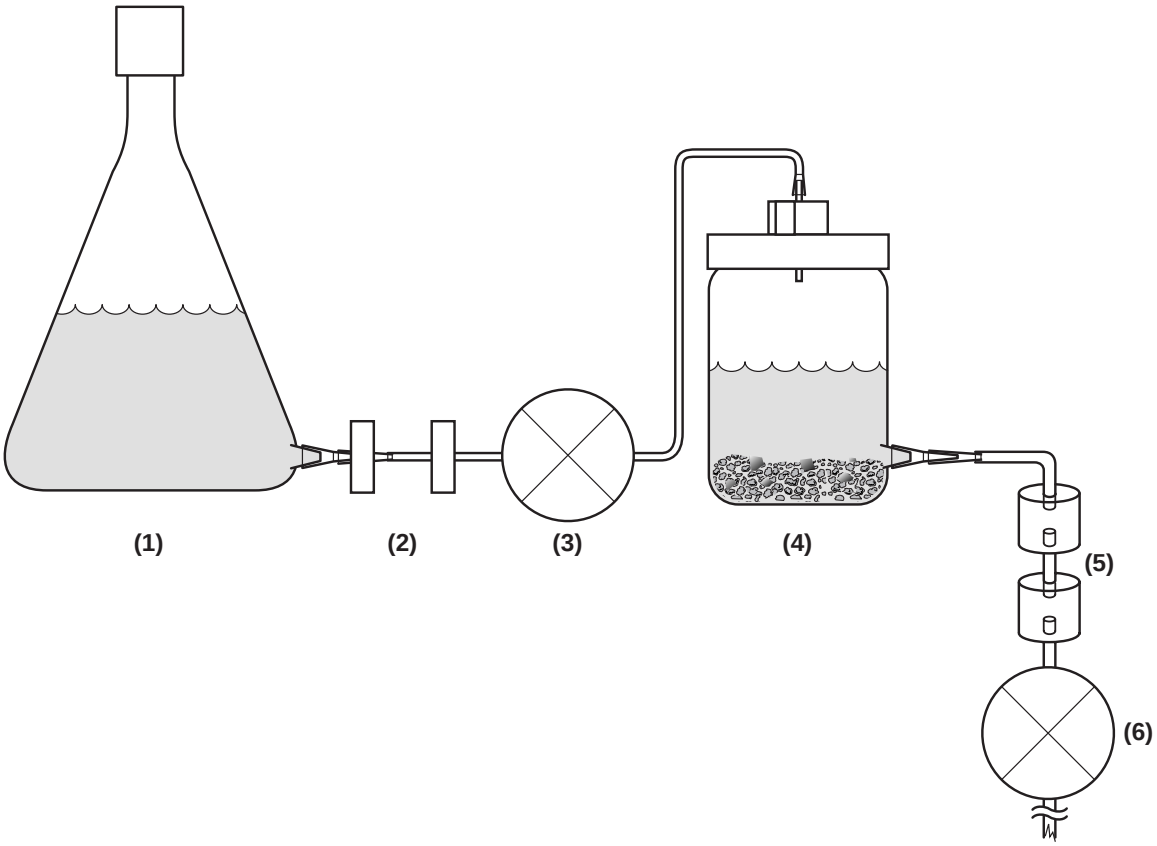

Figure 1. Configuration of microcosms. Each microcosm was composed of a 2 liter reservoir tank containing sterile media (1), that was fed through two 0.2 µm in-line filters (2), by means of a peristaltic pump (3), into a 500 ml modified spin flask that contained crushed YM tuff and coupon material (4). Media break tubes (5) on the outflow were used to prevent back-contamination, and the outflow rate was regulated by a second peristaltic pump (6).

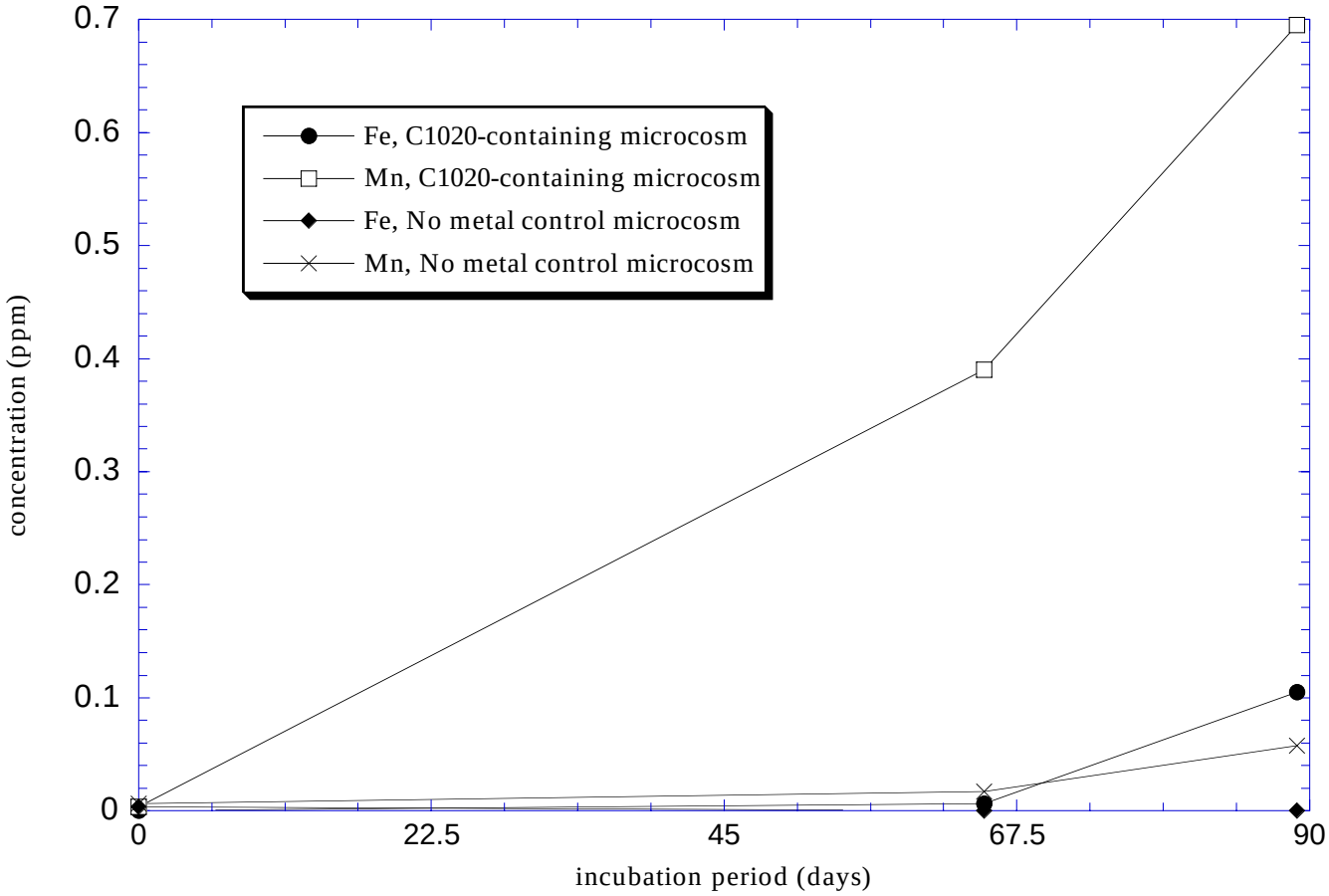

Figure 2. Solubilized Fe and Mn in microcosms containing either C1020 or no-metal controls. Fe and Mn concentrations in the 10XJ13 media were subtracted from these data. Results are an average of two trials.

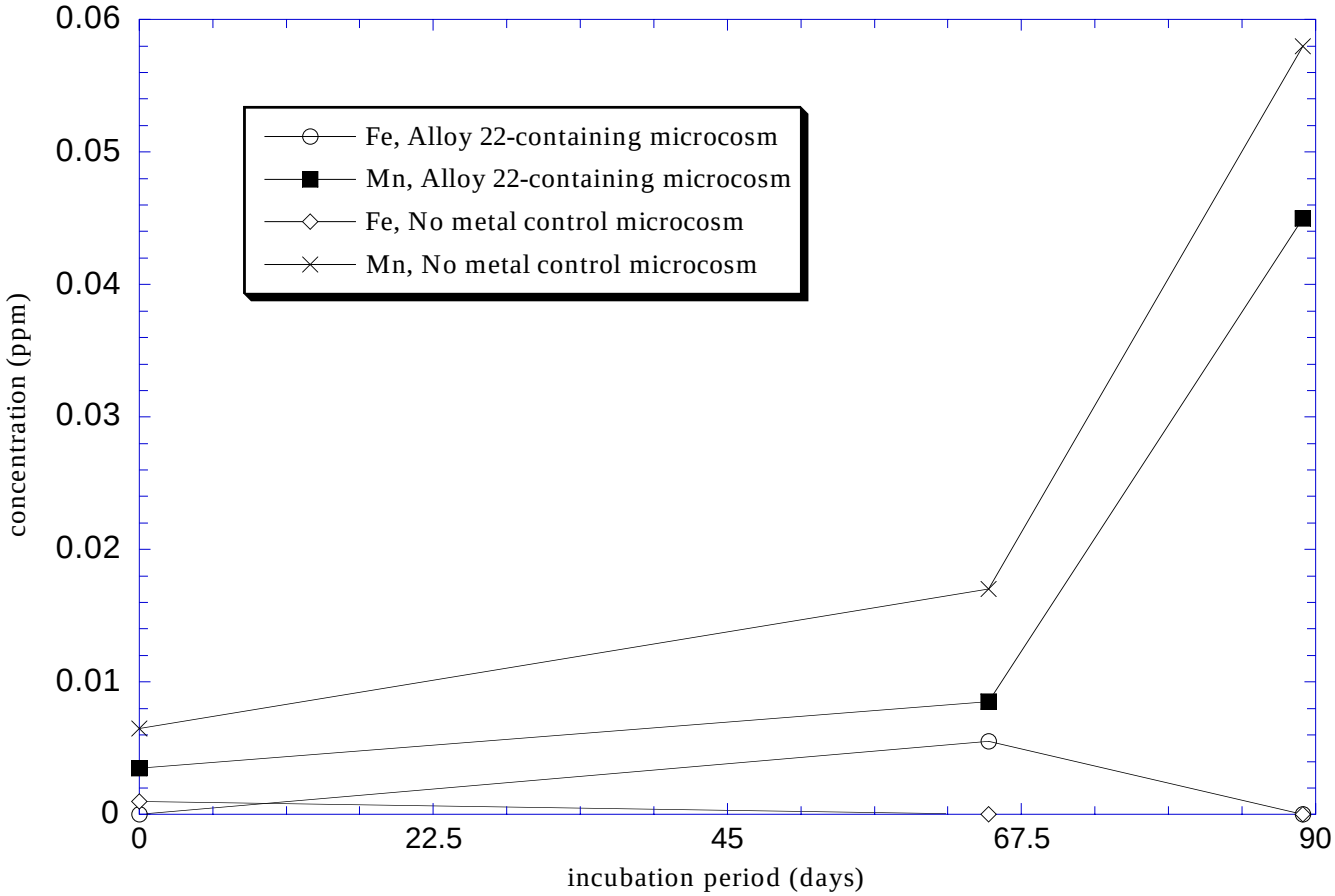

Figure 3. Solubilized Fe and Mn in microcosms containing either Alloy 22 or no-metal controls. Fe and Mn concentrations in the 10XJ13 media were subtracted from these data. Results are an average of two trials.

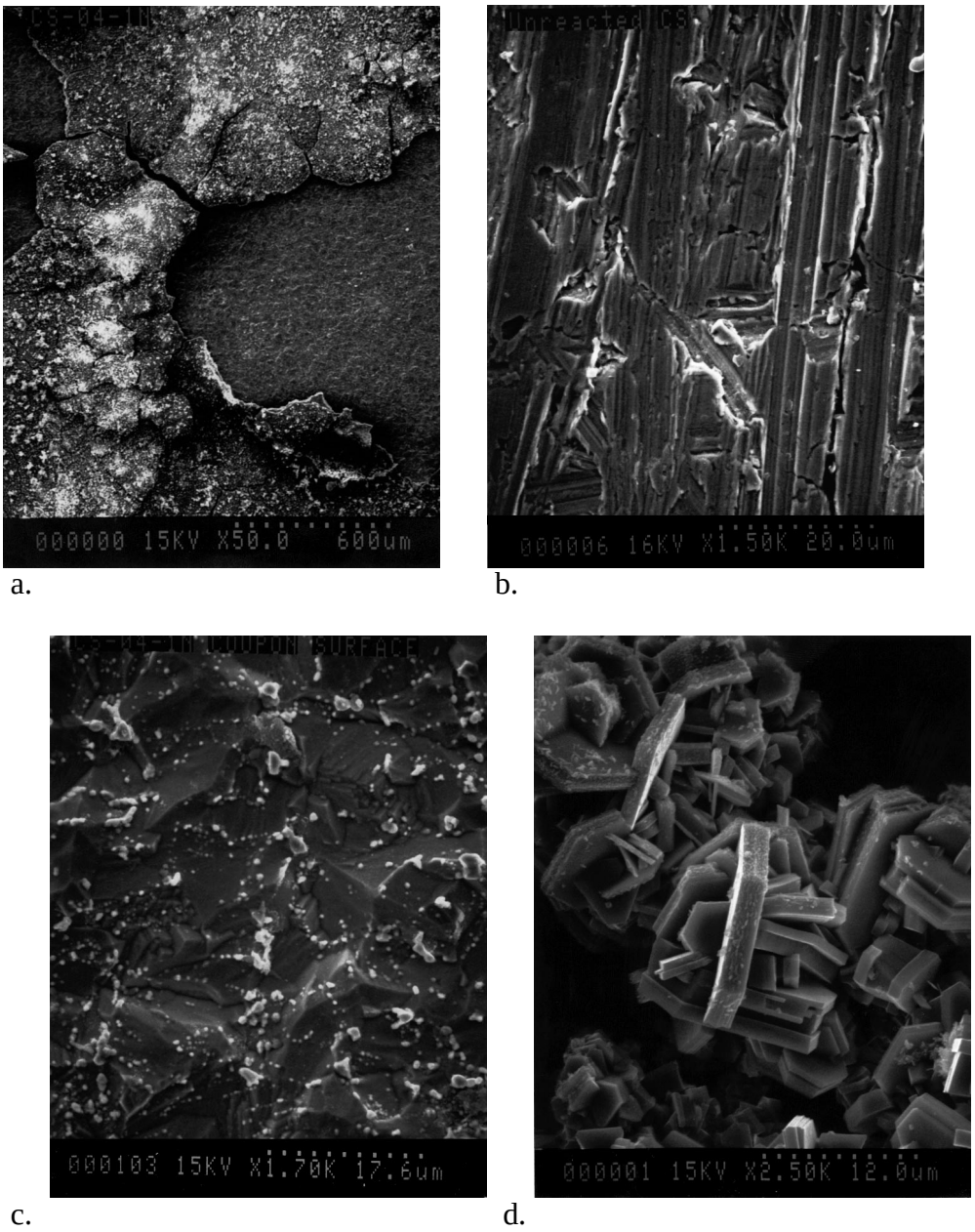

a. b. c. d.

Figure 4. SEM photomicrographs of C1020 coupons. Panel a) fractured, heterogeneous film overlaying microcosm-incubated surface; Panel b) unincubated/unexposed coupon surface; Panel c) isometric-shaped crystals of an Fe-bearing phase on microcosm-incubated coupon later identified by XRD as cohenite; Panel d) rhombohedron-shaped crystals composed of Ca and O on microcosm-incubated surface. Rod shaped bacteria are primarily attached to rhomb outer facets.

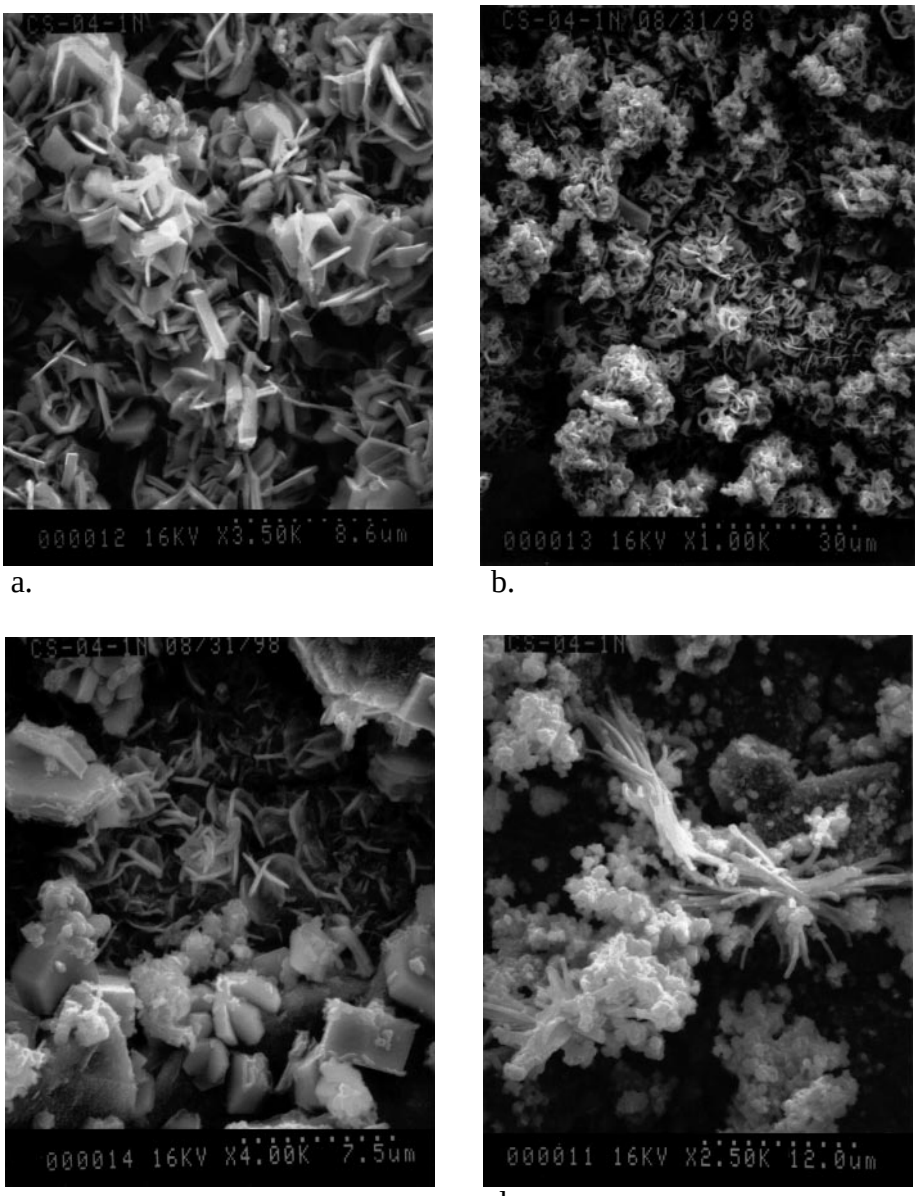

Figure 5. SEM photomicrographs of microcosm-incubated C1020 coupon films. Panels a & b) inward spiraling "honeycomb-like" particles composed of Fe, Si, and O; Panel c) co-occurrence of rhombohedrons, shown in Fig. 4, and "honeycombs"; Panel d) cable-like bundles composed of Ca, Si, and O, observed in minor amounts on coupon surface.

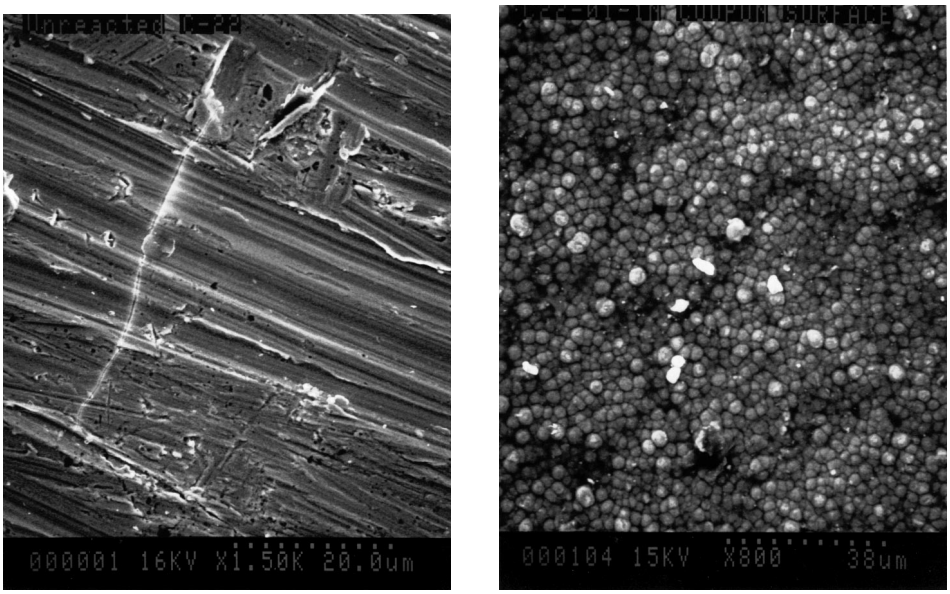

a. b.

Figure 6. SEM photomicrographs of the Alloy 22 coupon. Panel a) unreacted coupon surface; Panel b) coating of hemispherical particles composed of Cr and O observed on Alloy 22 after microcosm incubation.

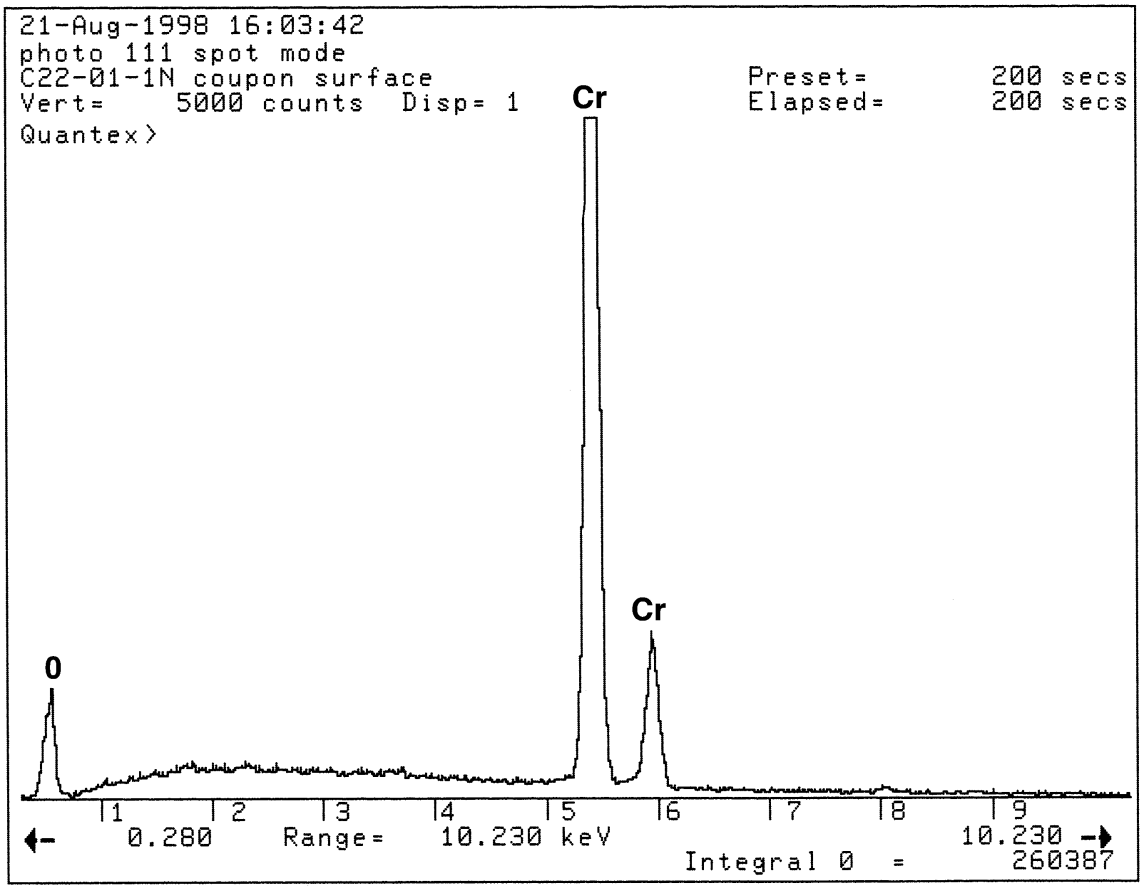

Figure 7. EDS spectrum of a microcosm-incubated Alloy 22 surface indicates that the film is composed of Cr and O.